



Cite this: *CrystEngComm*, 2021, **23**, 2606

On the supramolecular outcomes of fluorination of cyclohexane-5-spirohydantoin derivatives†

Kristina Gak Simić,^a Ivana Đorđević,^b Anita Lazić,^a Lidija Radovanović,^a Marija Petković-Benazzouz,^c Jelena Rogan,^d Nemanja Trišović^d and Goran Janjić ^{*b}

The quantitative assessment of intermolecular interactions and their cooperative effects has been performed in spirohydantoin-based model compounds, 3-benzoyl-1,3-diazaspiro[4.5]decane-2,4-dione (**1**) and 3-(4-fluorobenzoyl)-1,3-diazaspiro[4.5]decane-2,4-dione (**2**), through single crystal X-ray crystallography and quantum chemical studies. In both crystal structures, molecules generate the same hydrogen-bonded centrosymmetric $R_2^2(8)$ synthon. The extended supramolecular architectures depend on the C–H \cdots O, C–H \cdots π , stacking interactions and parallel interactions at large offsets, which lead to molecular sheets and further, with the assistance of the C–H \cdots F interaction in the case of **2**, to three-dimensional networks. Electrostatic potential maps have indicated that formation of the intermolecular F \cdots F interaction in the crystal structure of **2** results in a new region with a larger surface area and a higher negative potential in comparison to the individual fluorine atoms. Establishment of this interaction leads to strengthening of the interaction of one of the fluorine atoms with a third molecule from the environment which does not interact with both of them. When this third molecule interacts with both fluorine atoms simultaneously, the calculations have shown that the effect of strengthening of the individual interactions due to formation of the F \cdots F interaction is absent.

Received 19th December 2020,
Accepted 19th February 2021

DOI: 10.1039/d0ce01841d

rsc.li/crystengcomm

Introduction

Over the past two decades introduction of the fluorine atom into an organic molecule has been recognized as a routine strategy to address many challenges encountered in drug design and development.¹ Owing to its resemblance to hydrogen, high electronegativity and low polarizability, the fluorine atom as a substituent at the specific site can simultaneously influence many important properties of a drug candidate, including control of conformation, improvement of metabolic stability, modulation of pK_a , lipophilicity and protein binding affinity.¹ Because of this, a number of compounds based on scaffolds with fluorine have

been synthesized and clinically evaluated, so today 20–25% of marketed drugs contain at least one fluorine atom in their structures.^{1b} A need to balance processability, stability and bioavailability of drugs has motivated identification of their various polymorphs. Namely, the dissolution rate and oral absorption of poorly water-soluble drugs are determined by the physical state, while the crystal morphology can influence possibility of formulation of different solid dosage forms. A thorough understanding of the strength and directional preferences of diverse intermolecular interactions enable to control and predict development of the crystal structure. Having in mind the frequent occurrence of fluorine in many drugs, its participation in the formation of these interactions have been widely investigated.² Although individually weak, the total energy of these interactions can become significant.

In contrast to anionic fluoride, the capability of the C–F group to form hydrogen bonds has been questioned due to the low proton affinity and its inability to modify this by intramolecular electron delocalization.³ However, when the carbon acidity is at least at the level of fluorobenzenes and competing acceptors such as oxygen or nitrogen are absent, the C–F \cdots H–C interactions exhibit the directional characteristics of weak hydrogen bonds.⁴ Additionally, a Cambridge Structural Database (CSD)⁵ search has offered a conclusion that fluorine from the C(sp³)–F group is a better

^a Innovation Centre of the Faculty of Technology and Metallurgy, Karnegijeva 4, 11120 Belgrade, Serbia

^b Institute of Chemistry, Technology and Metallurgy, National Institute of the Republic of Serbia, University of Belgrade, Njegoševa 12, 11001 Belgrade, Serbia. E-mail: goran.janjić@ihm.bg.ac.rs

^c Faculty of Physics, University of Belgrade, Studentski trg 12, 11001 Belgrade, Serbia

^d Faculty of Technology and Metallurgy, University of Belgrade, Karnegijeva 4, 11120 Belgrade, Serbia

† Electronic supplementary information (ESI) available. CCDC 2045907 and 2045908. For ESI and crystallographic data in CIF or other electronic format see DOI: 10.1039/d0ce01841d

hydrogen bond acceptor than fluorine from the C(sp²)-F group.⁶ Loader *et al.* have examined the asymmetry of bifurcation in (C-F)₂⋯H-C bifurcated hydrogen bonds.⁷ Although asymmetry in distance does not require asymmetry in angle and *vice versa*, a geometric analysis of these hydrogen bonds has indicated a preference for symmetrically bifurcated interactions.

When compared with the other halogens, the F⋯F interactions have been regarded as controversial. The anisotropy of repulsion has a greater effect on short interatomic contacts in lighter halogen than attraction caused by weak polarization, which dominates the Br⋯Br and I⋯I interactions.⁸ The results of the energy decomposition have shown that electrostatic and dispersion energies have similar contribution to the total interaction energy and both overcome the repulsive component at distances greater than 3.0 Å.⁹ Regarding their stereochemical characteristics, Ramasubbu *et al.* have identified two types of angular preferences around the halogen centres.¹⁰ Namely, a “side-on” approach, nearly normal to the C-X bond, is not necessarily stabilizing and it is caused by close packing (type I), while a polarization of halogen atoms results in a “head-on” approach, behind the C-X bond (type II). Although the majority of the C-F⋯F-C interactions is of type I, Barcelo-Oliver *et al.* have suggested that they are not caused by the close packing only.¹¹ Based on quantum chemical calculations of model dimers of hexafluorobenzene, Karnoukhova *et al.* have confirmed that the most favorable is the interaction with C-F⋯F-C angles of 90° and the interaction energy being around -2.7 kcal mol⁻¹.¹² The interaction of type II with angles equal to 90° and 180° has almost two times lower energy, while the least favorable is the linear configuration. Bauzá and Frontera have demonstrated the capability of metal coordination, hydrogen and halogen bonding interactions to electrostatically enhance F⋯F interactions involving the aromatic fluorine atoms which leads to significant cooperative effects.¹³ An analysis of the crystal structure of compounds with a perfluorinated chain has enabled to identify an additional three point type of the C-F⋯F-C interaction between one fluorine atom from one molecule and two fluorine atoms from a neighboring molecule with the interaction energy ranging from 1 to 20 kcal mol⁻¹.¹⁴

In our previous paper,⁹ we have shown that the shift of the electron density in the area of the F⋯F interaction leads to formation of a new region with a larger surface area, a higher negative potential, and, hence, a more pronounced accepting ability. This new region has a greater ability to build simultaneous intermolecular interactions with species from the environment, thus compensating for the reduction of the accepting capacity of the neighboring groups in the molecule. Here, we present the synthesis and determination of the crystal structure of two derivatives of cyclohexane-5-spirohydantoin (1,3-diazaspiro[4.5]decane-2,4-dione) where the benzoyl or 4-fluorobenzoyl group is introduced in position 3 of the heterocyclic ring (Fig. 1). Hydantoin is an

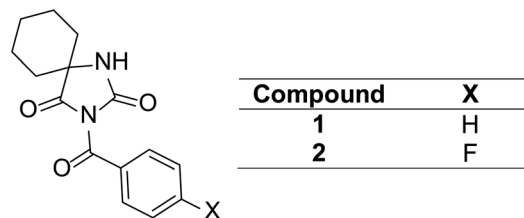


Fig. 1 Chemical structures of 3-benzoyl-1,3-diazaspiro[4.5]decane-2,4-dione (1) and 3-(4-fluorobenzoyl)-1,3-diazaspiro[4.5]decane-2,4-dione (2).

important scaffold present in many biologically active compounds and drugs, including blockbuster such as phenytoin(5,5-diphenylhydantoin, anticonvulsant), nilutamide(5,5-dimethyl-3-(4-nitro-3-(trifluoromethyl)phenyl)hydantoin, antineoplastic hormonal agent), nitrofurantoin(1-((Z)-((5-nitrofuranyl)methylidene)amino)hydantoin, antibiotic) and β-D-glucopyranose spirohydantoin (glycogen phosphorylase inhibitor).¹⁵ Notably, spirohydantoin have been identified as a class of highly efficient, short-acting prolyl hydroxylase 1-3 inhibitors causing a robust erythropoietin upregulation *in vivo* in multiple preclinical species.¹⁶ A spirohydantoin derivative, BMS-688521, has been recognized as a potent antagonist of the interaction between integrin leukocyte function associated antigen-1 and intercellular adhesion molecules and further advanced into clinical trials.¹⁷

Although the primary motifs, which constitute the backbone of the supramolecular structure of hydantoin derivatives, are governed by hydrogen bonding, special attention in this work has been paid to the changes in the supramolecular structures caused by replacement of the hydrogen atom by the fluorine atom. An emphasis has been given to the quantitative assessment of intermolecular interactions involving fluorine, particularly the C-H⋯F and F⋯F interactions, and the cooperative effect in systems dominated by hydrogen bonding. A mutual influence of the individual cyclic fragments of 1 and 2 has been investigated and supported by a CSD survey. Having in mind versatile biological activities of hydantoin derivatives, especially spirohydantoin, it is expected that the obtained results will help in affording guidelines for design of supramolecular assemblies for the applications in the life sciences.

Results and discussion

Molecular structures

Compounds 1 and 2 crystallize in the triclinic *P* $\bar{1}$ space group with *Z* = 2 (Fig. S1,† Table 1). In 2, the unit cell parameter *a* is shorter than the corresponding parameter in 1 (for around 0.3 Å), whereas the parameters *b* and *c* are longer (for around 0.6 Å), which results in the larger unit cell volume of 2 than of 1 (for *ca.* 3%).

Table 1 Crystallographic and refinement data for **1** and **2**

Compound	1	2
Formula	C ₁₅ H ₁₆ N ₂ O ₃	C ₁₅ H ₁₅ FN ₂ O ₃
Molecular weight/g mol ⁻¹	272.30	290.29
Crystal system	Triclinic	Triclinic
Space group	<i>P</i> $\bar{1}$	<i>P</i> $\bar{1}$
<i>a</i> /Å	6.3079(13)	5.9981(12)
<i>b</i> /Å	10.573(2)	11.148(2)
<i>c</i> /Å	11.415(2)	12.073(2)
α /°	67.21(3)	108.98(3)
β /°	78.84(3)	101.57(3)
γ /°	76.16(3)	105.27(3)
<i>V</i> /Å ³	677.1(3)	699.3(3)
<i>Z</i>	2	2
<i>D</i> _c /g cm ⁻³	1.336	1.379
μ /mm ⁻¹	0.094	0.106
<i>F</i> (000)	288	304
Crystal size/mm	0.75 × 0.25 × 0.18	0.72 × 0.30 × 0.11
θ range/°	3.45–25.34	3.30–25.35
Limiting indices	–7 ≤ <i>h</i> ≤ 7 –12 ≤ <i>k</i> ≤ 10 –13 ≤ <i>l</i> ≤ 13	–7 ≤ <i>h</i> ≤ 7 –10 ≤ <i>k</i> ≤ 13 –14 ≤ <i>l</i> ≤ 13
Measured reflections	5159	4747
Independent reflections	2484	2559
Reflections with <i>I</i> > 2σ(<i>I</i>)	1919	1812
<i>R</i> _{int}	0.0194	0.0189
Final <i>R</i> indices [<i>I</i> > 2σ(<i>I</i>)]	<i>R</i> ₁ = 0.0606 <i>wR</i> ₂ = 0.1620 ^a	<i>R</i> ₁ = 0.0482 <i>wR</i> ₂ = 0.1073 ^b
<i>R</i> indices (all data)	<i>R</i> ₁ = 0.0772 <i>wR</i> ₂ = 0.1746	<i>R</i> ₁ = 0.0733 <i>wR</i> ₂ = 0.1198
<i>S</i>	1.058	1.031
Parameters	181	190
$\Delta\rho_{\max}$, $\Delta\rho_{\min}$ /e Å ⁻³	0.295, –0.175	0.137, –0.174

^a $w = 1/[\sigma^2(F_o^2) + (0.1081P)^2 + 0.0399P]$ where $P = (F_o^2 + 2F_c^2)/3$. ^b $w = 1/[\sigma^2(F_o^2) + (0.0549P)^2 + 0.0354P]$ where $P = (F_o^2 + 2F_c^2)/3$.

Representative ORTEP diagrams of **1** and **2** are shown in Fig. 2. Selected molecular geometry parameters of the investigated compounds are presented in Table S1.†

As expected, the central hydantoin moiety is essentially planar and nearly perpendicular to the mean plane of the cyclohexyl ring (the corresponding dihedral angles of 88.7° in **1** and 89.7° in **2**). An increase in the dihedral angle between the hydantoin and phenyl rings, separated by a carbonyl group, is observed in **2** (81.9°) relative to that in **1** (53.8°), possibly caused by electronic effects of the fluorine atom.

The bond lengths and angles in the hydantoin ring are in a good agreement with the values found in the related cycloalkane-5-spirohydantoin. ¹⁸ A shortening of the C2–N3 and N3–C4 bonds in **2** relative to those in **1** reflects the transmission of electronic effects of the fluorine atom. Introduction of this atom also causes enlargement of the N3–C11 bond and shortening of C11–C12 bond in the bridge. Bending of the C11=O3 carbonyl bond is somewhat larger in **2** than **1**. Namely, the C12–C11–O3 angle is greater than the N3–C11–O3 angle in both crystal structures.

Hirshfeld surface analysis

To quantify the intermolecular interactions present within the crystal structures of **1** and **2**, the Hirshfeld surface and subsequent fingerprint plots have been initially calculated. ^{18c,19} The Hirshfeld surfaces mapped over *d*_{norm} are illustrated in Fig. S2.† The bright-red spots show the N–H⋯O hydrogen bonds, while faint-red spots in **2** are due to the comparatively weak C–H⋯O interaction.

A simple visual inspection shows that the fingerprint plots of **1** and **2** are different (Fig. S3 and S4.†). As expected, the

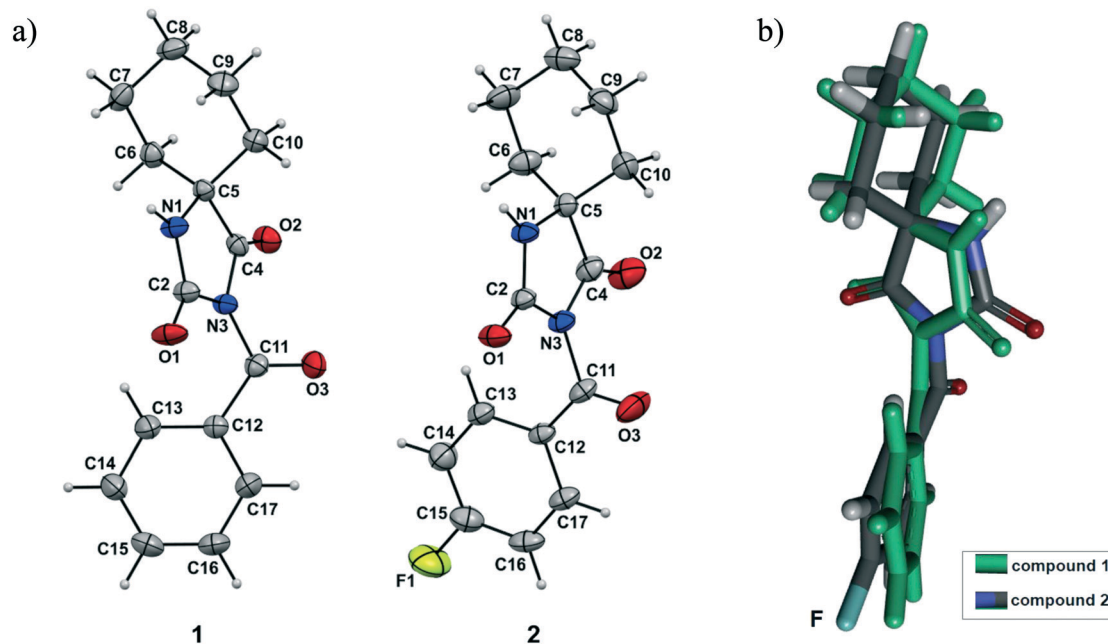


Fig. 2 a) ORTEP diagram of **1** and **2** with the atom numbering scheme. The thermal ellipsoids are drawn at the 50% probability level, b) overlay of **1** (green) and **2**.

H···H, H···O, H···C and especially H···F interactions in the case of **2** have the highest contributions (Fig. S5†). Namely, the H···H contribution in **2** is for 16.3% lower than in **1**, while the contributions from the other intermolecular contacts are similar. The shortest H···H interactions are depicted as a pair of broad spikes at $d_e + d_i \sim 2.2\text{--}2.4 \text{ \AA}$, whereby a subtle splitting typical for a three-atom contact can be observed.¹⁹ The H···O interactions with a contribution of around 30% have a symmetrical distribution of points, whereby N–H···O hydrogen bonds are represented by a pair of spikes at the bottom left of the fingerprint plot.¹⁹ The H···C contacts, as the measure of the C–H··· π interactions, contribute with 14% to the overall fingerprint plot and are presented as scattered wings. The presence of a pair of two smaller spikes at $d_e + d_i \sim 2.6\text{--}2.8 \text{ \AA}$ in the fingerprint plot arises from short intermolecular H···F contacts with the contribution of 12.6%. The contributions of other contacts to the Hirshfeld surface seem to be negligible.

Crystal packing

The lattice energies of both crystal structures have been calculated using PIXEL²⁰ and further partitioned into coulombic, dispersive, polarization and repulsive factors (Table S2†). As already observed for structurally-related cyclohexane-5-spirohydantoin derivatives,^{18b} dispersion, rather than coulombic or polarization, has the dominant contribution to the total lattice energy.

The evolution of the crystal structure has been further considered in terms of different dimeric motifs as the basic building blocks, which are associated with the presence of intermolecular interactions. CrystalExplorer has been used to roughly estimate the distribution patterns of the interaction energy between a pair of molecule (electrostatic, polarization, dispersion and repulsion, Tables S3 and S4†).²¹

To obtain more accurate values of interaction energies, the calculations at TPSSH-D3/def2TZVP level have been performed in the Gaussian09 program. Concerning

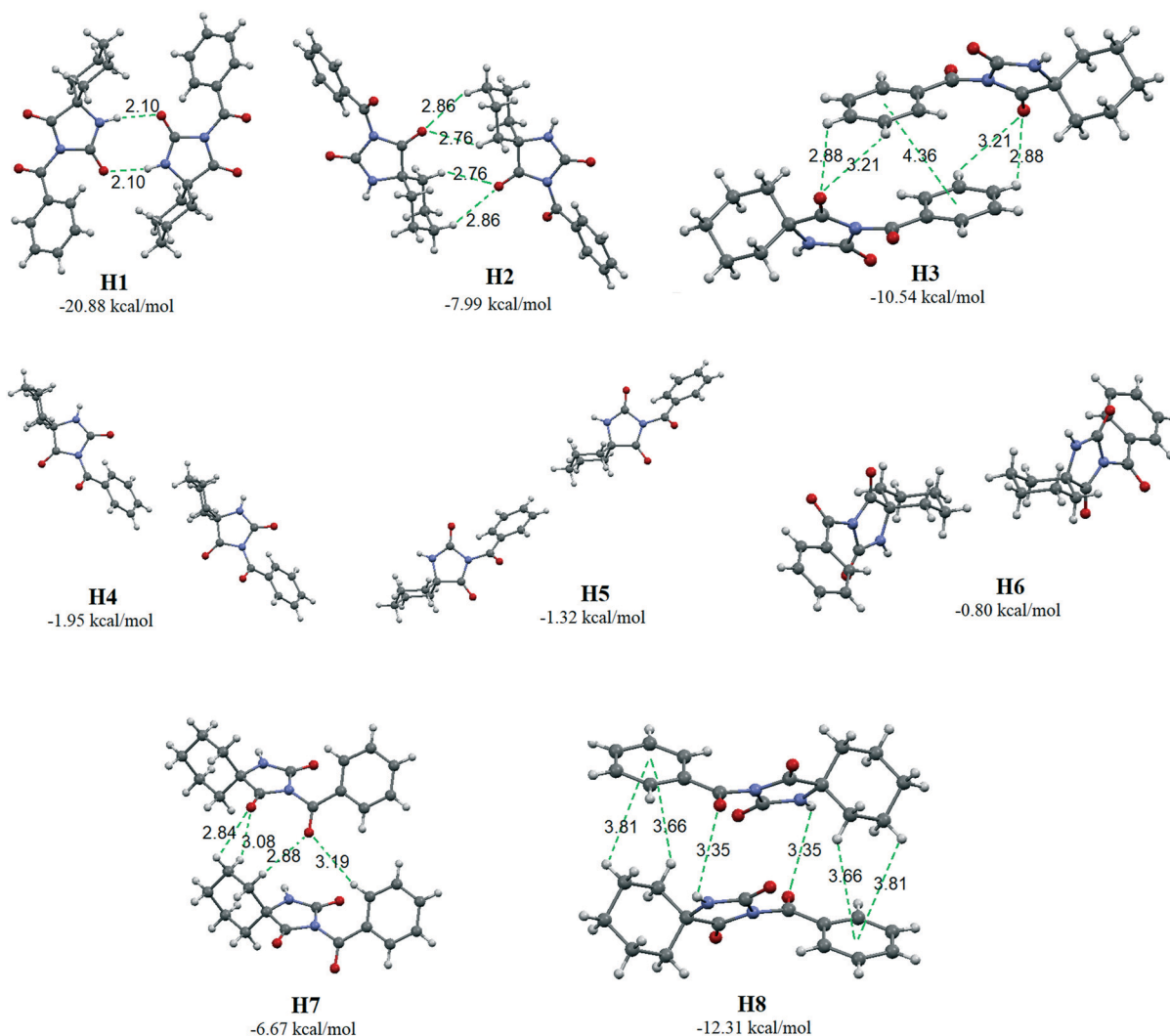


Fig. 3 Dimeric motifs H1–H8 extracted from the crystal structure of **1** with their interaction energies.

compound **1**, the structures of these dimeric motifs and the corresponding interaction energies (ΔE) are presented in Fig. 3. The molecules associate into a hydrogen bonded centrosymmetric $R_2^2(8)$ dimeric motif (motif H1, $\Delta E = -20.88$ kcal mol $^{-1}$). This motif, together with the motif H2 ($\Delta E = -7.99$ kcal mol $^{-1}$) of bifurcated C(sp 3)-H \cdots O hydrogen bonds pointing towards the O2 atom, builds a supramolecular chain

running along the c -axis. On the other side, the double chain along the b -axis is generated by the action of the motifs H1 and H3.

The relative position of the molecules in the motif H3 ($\Delta E = -10.54$ kcal mol $^{-1}$) is such that, besides two pairs of the bifurcated C(sp 2)-H \cdots O hydrogen bonds, there is a parallel interaction at a large offset (PILO, Cg \cdots Cg distance 4.362 Å).

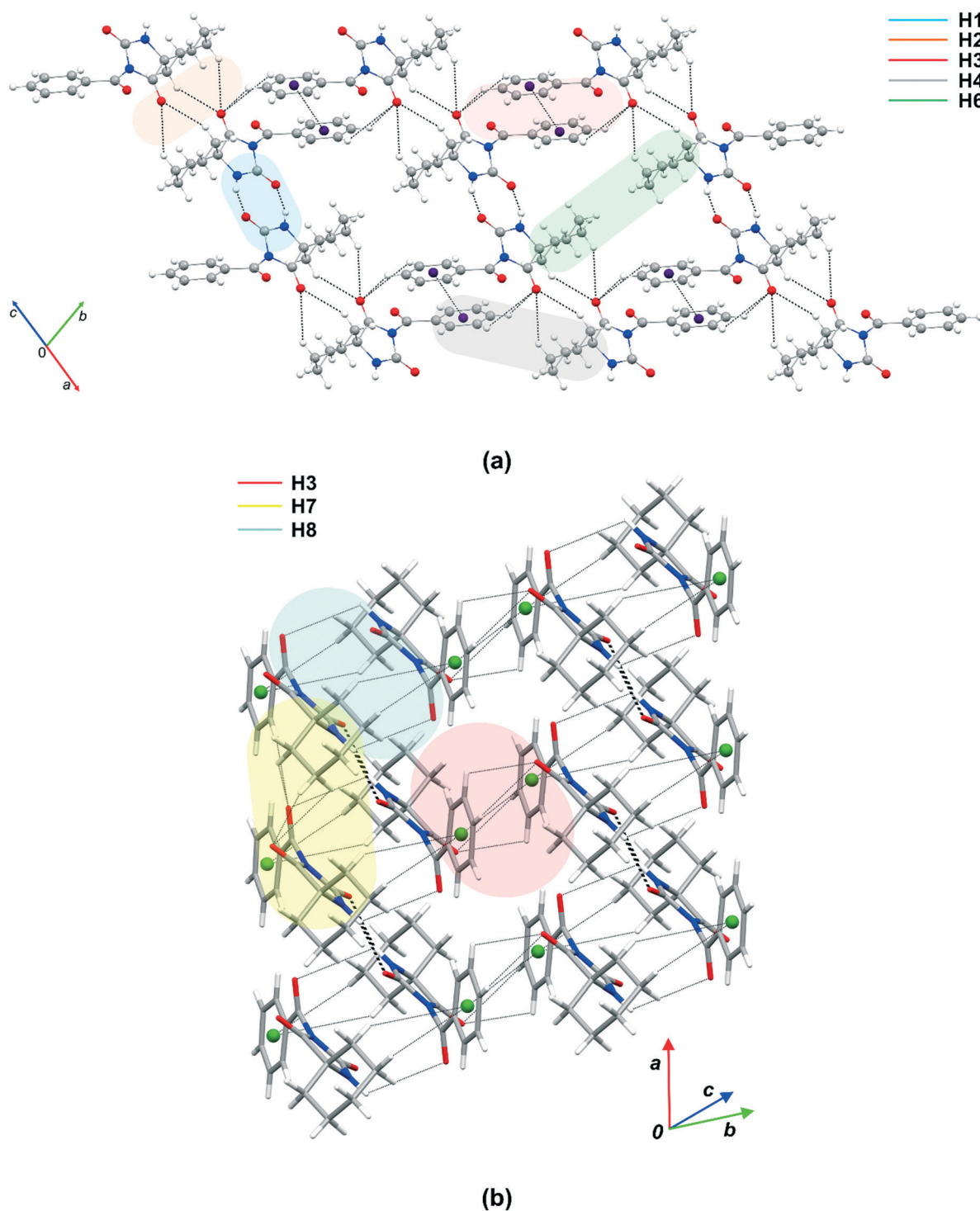


Fig. 4 Part of the crystal structure of **1** showing formation of a sheet (a) and a double chain (b).

Although weaker than $C(sp^2)-H\cdots\pi$ and stacking interactions with ΔE of about -2.9 kcal mol $^{-1}$, PILOs between two benzene molecules (with ΔE of about -2.0 kcal mol $^{-1}$) are more frequent in the crystal structures than the these two. Namely, this interaction is responsible for the higher interaction energy of the motif H3 relative to the motif H2.²²

The interaction between the chains, which involves motifs H4 and H6, then produces a continuous sheet parallel to the *bc*-plane (Fig. 4a). An additional stabilization in motifs H4, generated by translation, and H6, generated by inversion, is provided over hydrophobic interactions between the cyclohexyl and phenyl rings (ΔE being -1.95 and -0.80 kcal mol $^{-1}$, respectively). Here, hydrophobic interactions are understood as an attraction between hydrophobic fragments (cyclohexyl and aromatic rings), which do not involve the π -system of the phenyl rings.

Besides the interaction energy, symmetry seems to be an important factor in these sheets. The sheets are then linked into a three-dimensional framework by means of the motifs H7 and H8. The molecules within the motif H1 are linked into a double chain parallel to the *a*-axis by means of the motifs H7 and H8. The motif H7 ($\Delta E = -6.67$ kcal mol $^{-1}$), generated by translation, involves two pairs of $C-H\cdots O$ interactions sharing the same acceptors (O2 and O3). Paired $N-H\cdots O$ hydrogen bonds where O3 acts as an acceptor in a combination with two pairs of $C(sp^2)-H\cdots\pi$ interactions create the motif H8 ($\Delta E = -12.31$ kcal mol $^{-1}$). These double chains are themselves linked, among others, by hydrophobic contacts of the motif H5 ($\Delta E = -1.32$ kcal mol $^{-1}$).

The structures of dimeric motifs extracted from the crystal packing of **2** and the corresponding interaction energies are presented in Fig. 5. Again, as in **1**, the molecules of **2** are

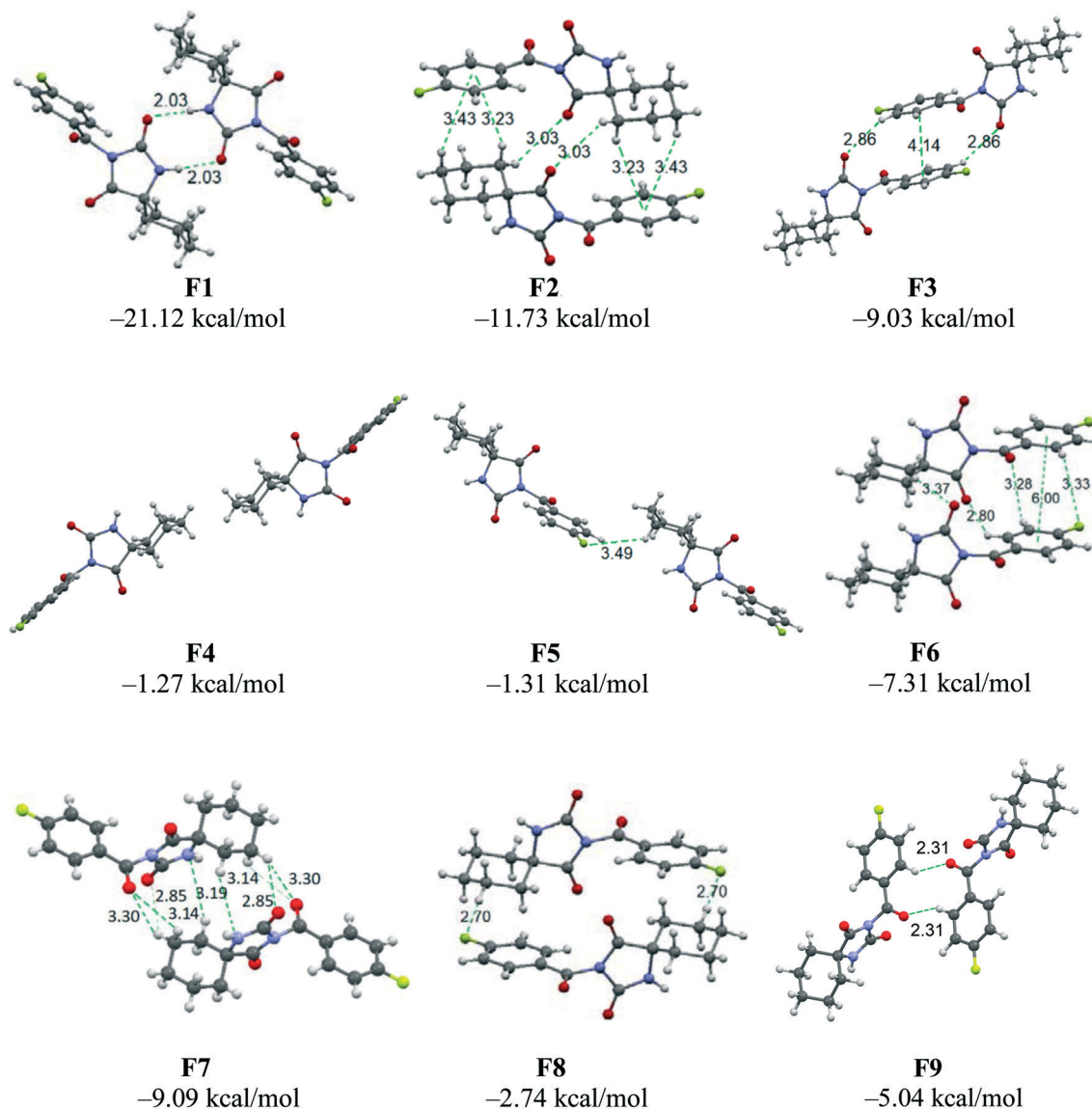


Fig. 5 Dimeric motifs F1–F9 extracted from the crystal structure of **2** with their interaction energies.

linked by paired N-H \cdots O hydrogen bonds into a centrosymmetric R $_2^2$ (8) dimer unit (motif F1, $\Delta E = -21.12$ kcal mol $^{-1}$). In this case, the N-H \cdots O bond is shorter than the one within the isostructural motif of **1** (2.10 and 2.03 Å for **1** and **2**, respectively), thus resulting in slightly higher interaction energy. As expected, the shorter N-H \cdots O bond in **2** also results in an increase of both electrostatic and repulsion terms (Tables S3 and S4 †). Two weak C(sp 3)-H \cdots O hydrogen bonds (3.23 and 3.43 Å) together with two C(sp 3)-H \cdots π interactions with the distance between the H atom and the π plane of 3.03 Å link molecules into the motif F2 ($\Delta E = -11.73$ kcal mol $^{-1}$). The alternation of the motifs F1 and F2 further results in formation of a chain running along the *b*-axis.

When comparing interaction energy of the motifs H2 and F2, both oriented along the same direction, an important difference resulting from the fluorination of the phenyl ring can be noticed. In H2, both cyclohexyl rings interact with the hydantoin moieties and form the C(sp 3)-H \cdots O hydrogen bonds. On the other side, in F2, the cyclohexyl rings are shifted towards the phenyl rings, thus resulting in the C(sp 3)-H \cdots π interactions. The net result is the higher interaction of the motif F2 than ΔE of the motif H2. This indicates that the fluorinated phenyl ring establishes stronger C(sp 3)-H \cdots π interactions than the non-substituted one.

As in **1**, symmetry controls the molecular assembly, *i.e.*, development of the crystal packing. The chains are linked by motifs F3, F4 and F5 and thus formed a sheet (Fig. 6). The motif F4 is highly dispersive; the hydrophobic interactions involve the cyclohexane rings of the paired molecules ($\Delta E = -1.27$ kcal mol $^{-1}$). In the motif F5 ($\Delta E = -1.31$ kcal mol $^{-1}$), which is generated by translation, the mean plane of the cyclohexyl ring of one molecule is nearly parallel to the phenyl ring of another molecule, so interaction between them can be considered as a PILO (Cg \cdots Cg distance of 6.02 Å). This motif also involves a C(sp 2)-H \cdots F interaction. In the motif F3 ($\Delta E = -9.03$ kcal mol $^{-1}$), a pair of molecules is linked by two C(sp 2)-H \cdots O hydrogen bonds and a stacking interaction of the phenyl rings (Cg \cdots Cg distance of 4.14 Å). This motif can be regarded as a governing force in the assembly process, while the motifs F4 and F5 resulted from the packing.

Finally, the motifs F6, F7, F8 and F9 join together neighboring sheets into a three-dimensional network. Two translation-related molecules in the motif F6 ($\Delta E = -7.31$ kcal mol $^{-1}$) are linked by pairs of C(sp 3)-H \cdots O and C(sp 2)-H \cdots F hydrogen bonds as well as a PILO (Cg \cdots Cg distance of 6.00 Å). The molecules in the motif F7 ($\Delta E = -9.09$ kcal mol $^{-1}$) participate in a pair of bifurcated C(sp 3)-H \cdots O hydrogen bonds and a pair of C(sp 3)-H \cdots N hydrogen bonds. The motif F8 ($\Delta E = -2.74$ kcal mol $^{-1}$) contains two C(sp 3)-H \cdots F

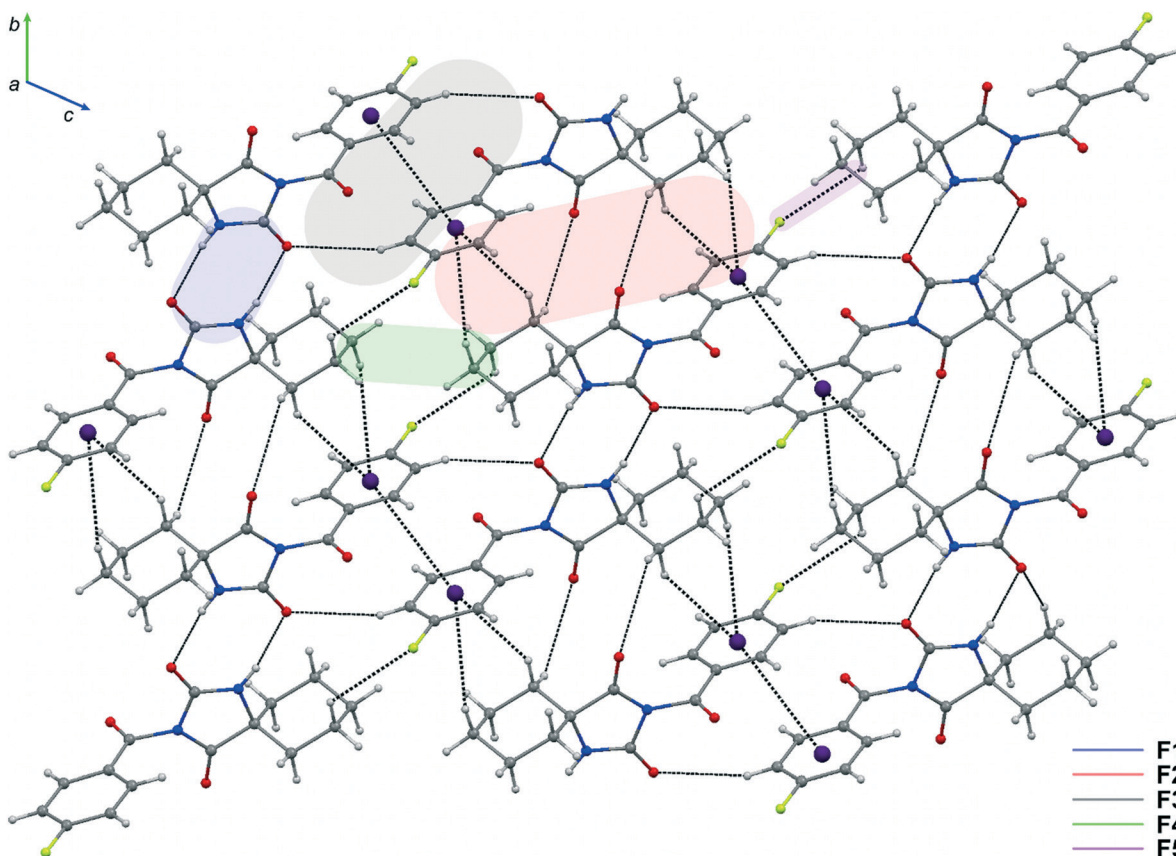


Fig. 6 Part of the crystal structure of **2** showing formation of a sheet.

hydrogen bonds which result in formation of a centrosymmetric $R_2^2(24)$ ring. In the motif F9 ($\Delta E = -5.04$ kcal mol⁻¹), the molecules are linked through a pair of C(sp²)-H...O hydrogen bonds, thus resulting in a $R_2^2(10)$ ring.

When comparing **1** and **2**, changes in the unit cell parameters might result from differences in the total interaction energy of all the motifs oriented along the same axis, *i.e.*, the higher this interaction energy is, the more the dimension of the unit cell along this axis decreases.

In **1**, the molecule orientation along the *a*-axis is uniform and corresponds to the motif H7, with the distance between the centers of mass of 6.308 Å. There is no contact between the cyclohexyl rings in this case. In **2**, the molecules orientate along the *a*-axis similarly as in **1**, but are shifted more closely to each other. This can be presented by the motif F6. The shifting results in formation of a contact between the cyclohexyl rings and distancing of the cyclohexyl and hydantoin rings. The net result is an increase in the interaction energies. The molecules are closer to each other than in **1**, as reflected by the center of mass distance of 5.998 Å. The center of mass distances are equal to the values of *a* parameter of the corresponding unit cells. Hence, the decrease of 0.3 Å (relative to the center of mass distance in **1**) corresponds to the shortening of the unit cell parameter *a* of **2**.

Quantum chemical calculations on model systems derived from the cyclic units present in **1**

The analysis of the motifs (Fig. 3) used to describe the crystal packing of **1** has revealed that the hydantoin ring forms the largest number of contacts with the cyclohexyl ring (3 contacts; H2 and H7 motifs).

Here, under the contact we understand a group of intermolecular interactions between two cyclic fragments, whereby those of the bridging carbonyl group are ascribed to the phenyl ring. With another hydantoin ring (H1 and H8 motifs) and the phenyl ring (H3 motif), on the other side, the hydantoin ring establishes two contacts (Table S5†). Interactions between the hydantoin rings can be classified as N-H...O hydrogen bonds, while interactions with the cyclohexyl and phenyl rings are usually C-H...O interactions wherein the hydantoin carbonyl oxygen atom participates as an acceptor. On the other hand, the cyclohexyl ring has the highest affinity toward the phenyl ring (5 contacts; H4, H5, H7 and H8 motifs). There is only one contact wherein two cyclohexyl rings participate; it is the hydrophobic interaction. The phenyl ring, in addition to a high affinity toward the cyclohexyl ring and two contacts with the hydantoin ring, forms two contacts with other phenyl rings; one is a stacking interaction, while another one is a PILO.

The total interaction energy of one molecule with all surrounding molecules in the crystal structure of **1** has a value of -62.5 kcal mol⁻¹.

To determine the contribution of the individual cyclic fragments (phenyl, cyclohexyl and hydantoin), DFT

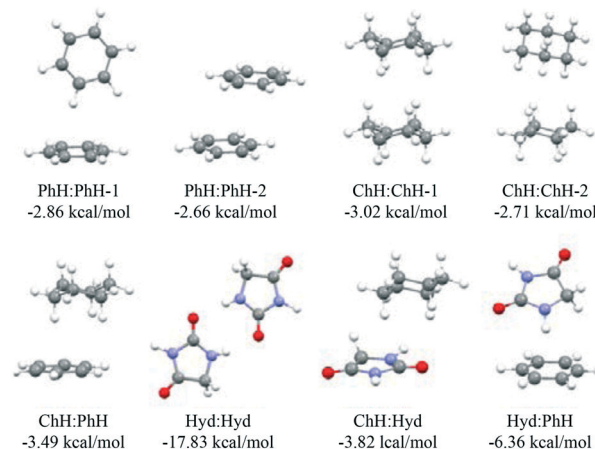


Fig. 7 The most stable structures of homo- and heterodimers of benzene, cyclohexane and hydantoin.

calculations have been performed on a model of dimer systems containing molecules of benzene (PhH), cyclohexane (ChH) or hydantoin (Hyd). The optimization has been applied on the initial structures, which has one of the following geometries: face-to-face, T-shaped, displaced, displaced with large offset or planar orientation. The representations of the initial and optimized structures with the assigned orientations and interaction energy are given in the ESI† (Tables S6–S11). The most stable orientations for individual homo- and heterodimeric systems are shown in Fig. 7.

It is well known that interaction energy of two benzene rings has two minima, one with the T-shaped geometry, corresponding to the C-H... π interactions (-2.86 kcal mol⁻¹) and another one with parallel displaced orientation, corresponding to stacking interactions (-2.66 kcal mol⁻¹). However, one another geometry of the benzene dimer has been identified, corresponding to a PILO (-1.98 kcal mol⁻¹). This is the most frequent orientation in the crystal structures (Fig. S6†).^{2,3}

In the case of the cyclohexane dimers (Table S7†), the starting face-to-face geometry has not changed after optimization convergence. When the T-shaped geometry and displaced geometry at large offset have been taken as the starting point in calculation, two T-shaped orientations are obtained. The face-to-face geometry of the cyclohexane dimer is more stable (Fig. 7, -3.02 kcal mol⁻¹) than the most stable T-shaped geometry of two cyclohexanes (Fig. 7, -2.71 kcal mol⁻¹). According to the calculated interaction energies, it can be concluded that the interactions associated with the parallel orientation of the benzene molecules are slightly weaker than the interactions with the parallel orientations of mean planes of the cyclohexane molecules (the cyclohexane mean plane containing the carbon atoms at positions 1, 2, 4 and 5 is observed), while interactions associated with the T-shaped geometry are slightly stronger in the case of the benzene dimers.

Replacement of one of the cyclohexane molecules with benzene has led to formation of ChH:PhH heterodimers,

which gave, after optimization, only one orientation (Table S9[†]) with the displaced geometry and interaction energy of $-3.49 \text{ kcal mol}^{-1}$ (Fig. 7). This points out that cyclohexane and benzene have higher affinities for heterodimers than homodimers. The conclusion is consistent with the data obtained from the crystal structure of **1**, which also confirms that the cyclohexane ring has a higher affinity for the phenyl ring than for another cyclohexane ring.

Fig. 7 shows the optimized hydantoin dimer – a planar system wherein these molecules form a pair of N–H \cdots O hydrogen bonds with the interaction energy of $-17.83 \text{ kcal mol}^{-1}$. This is the strongest interaction among the examined motifs. After optimization, the initial structures of ChH:Hyd heterodimer gave only one orientation (Table S10[†]), which corresponds to a displaced geometry with the interaction energy of $-3.82 \text{ kcal mol}^{-1}$ (Fig. 7). According to these calculations, it should be expected that the cyclohexyl group has a slightly higher affinity for the hydantoin ring than for the phenyl ring. However, cyclohexane is located above the hydantoin ring in the mentioned dimer (ChH:Hyd dimer, Fig. 7). In **1**, this position is sterically hindered by the cyclohexyl and aromatic moieties. In accordance with this, only orientations out of the ring, which contains the cyclohexyl group interacting with the carbonyl group, have been found here. The C–H \cdots O interactions are significantly weaker than interaction within the displaced geometry. Replacement of hydantoin with benzene (ChH:PhH) causes a slightly smaller decrease in interaction energy ($-3.49 \text{ kcal mol}^{-1}$).

Optimization of the initial geometries of Hyd:PhH dimers has led to several different orientations with the T-shaped geometry (Table S11[†]); the most stable among them ($-6.36 \text{ kcal mol}^{-1}$) is shown in Fig. 7. In this orientation, the molecules build N–H \cdots π hydrogen bond, which is further enhanced by a C–H \cdots O interaction. These calculations have implied that the phenyl group has a higher affinity toward the hydantoin ring than for the cyclohexane ring or another phenyl ring. However, this orientation (Hyd:PhH dimer, Fig. 7) does not occur in the crystal structure of **1**, because one N–H group has already been engaged in the formation of hydrogen bond, present in the motif H1, which is more energetically favorable. Only C–H \cdots O interactions between the hydantoin and phenyl rings have been found in the crystal structure of **1**. These interactions are weaker (energy about $-1.7 \text{ kcal mol}^{-1}$)²² not only than the stacking interactions between two benzene molecules ($-2.66 \text{ kcal mol}^{-1}$), but also than their PILO ($-1.98 \text{ kcal mol}^{-1}$).²³

Quantum chemical calculations on model systems derived from the cyclic units present in **2**

By analyzing the contacts of the individual rings in the crystal structure of **2** (Table S12[†]), it can be concluded that the hydantoin ring builds the largest number of contacts with the cyclohexyl ring (5 contacts; F2, F6, and F7 motifs), followed by those with the phenyl ring (3 contacts; F3 and F6

motifs). Although there is only one contact with another hydantoin ring (F1 motif), this contact (a pair of N–H \cdots O hydrogen bonds) is multiply stronger than the interactions with the other two rings – mainly C–H \cdots O interactions involving the hydantoin O atom. The cyclohexyl ring has no affinity towards the same ring (only 1 contact; a weak hydrophobic interaction in the motif F4). However, the cyclohexyl ring has the highest affinity toward the phenyl ring (7 contacts; motifs F2, F5, F7 and F8) and their interactions are very diverse (C–H \cdots π , C–H \cdots F and C–H \cdots O interactions involved) wherein the cyclohexane C–H groups act as donors. There are also three types of interactions between the aromatic rings: C–H \cdots π interaction, stacking interaction and PILO (motifs F3, F6 and F9). Introduction of the fluorine atom into the aromatic moiety results in an increase of the number of interactions with all, the hydantoin (3 contacts; motifs F3 and F6), cyclohexyl ring (7 contacts; motifs F2, F5, F7 and F8) and aromatic ring (3 contacts; motifs F3, F6, and F9).

The total interaction energy of one molecule with all molecules from the neighbourhood is slightly higher ($-68.6 \text{ kcal mol}^{-1}$) in the crystal packing of **2** than in the crystal packing of **1** ($-62.5 \text{ kcal mol}^{-1}$). This data indicates that fluorination of the aromatic ring increased the stability of the crystal structure. To determine the contribution of the interactions of the individual fragments (aromatic, cyclohexane and hydantoin) to the overall stability of the crystal structure, DFT calculations have been performed for the model systems of homodimers of fluorobenzene (PhF) and heterodimers containing the molecules of cyclohexane (ChH), fluorobenzene (PhF) or hydantoin (Hyd). The initial structures with face-to-face, T-shaped, displaced, displaced at a large offset or planar geometry have been optimized. Representations of the initial and optimized structures, with the appropriate geometry and interaction energies, are given in the ESI[†] (Tables S13–S15). The most stable geometries for the individual dimer systems are shown in Fig. 8.

Fluorination of the benzene ring has resulted in an increase in energy of the stacking interaction ($-3.68 \text{ kcal mol}^{-1}$, Fig. 8) and the C–H \cdots π interaction ($-3.24 \text{ kcal mol}^{-1}$,

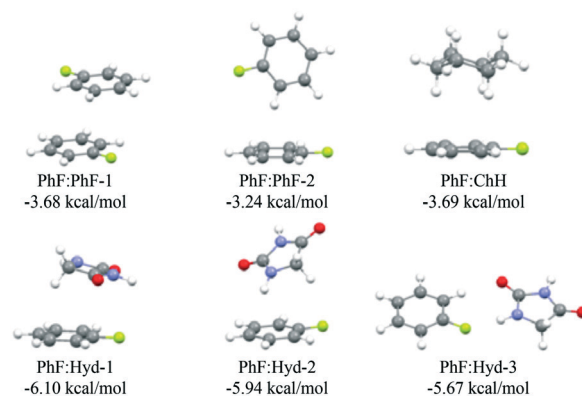


Fig. 8 The most stable structures of individual homo- and heterodimers involving fluorobenzene.

Fig. 8) when compared to unsubstituted benzene (Fig. 7). The increase is more pronounced for stacking interaction (about 1 kcal mol^{-1}). When optimizing the initial structures of the heterodimeric system, PhF:ChH (formed by replacing fluorobenzene with cyclohexane), in most cases, a dimer with the parallel displaced geometry is obtained with interaction energy of $-3.69 \text{ kcal mol}^{-1}$. In this case, interaction energy for these multifurcated C-H $\cdots\pi$ interactions is the same as the stacking interaction between two fluorobenzenes (PhF:PhF-1), but slightly higher than the C-H $\cdots\pi$ interaction between these two molecules (PhF:PhF-2). This indicates that cyclohexane is a better C-H donor than benzene and fluorobenzene. In the most stable orientation of the PhF:ChH dimer, in addition to the C-H $\cdots\pi$ interaction, there is also the C-H \cdots F interaction. This is probably a reason why the PhF:ChH dimeric system is more stable than the most stable ChH:PhH dimeric system wherein benzene and cyclohexane interact. Interestingly, one of the optimized structures with the PhF:ChH dimer, with a PILO, has higher energy ($-2.13 \text{ kcal mol}^{-1}$, Table S14[†]) than the system of the benzene dimer ($-1.98 \text{ kcal mol}^{-1}$).²² Replacement of one fluorobenzene molecule in PhF:PhF dimer with a hydantoin molecule (PhF:Hyd heterodimer) has led to an increase in the interaction energy ($-6.10 \text{ kcal mol}^{-1}$, Fig. 8), which is almost twice as high as the energy of PhF:PhF dimer with parallel displaced geometry (PhF:PhF-1). The PhF:Hyd-2 dimer with the T-shaped geometry ($-5.94 \text{ kcal mol}^{-1}$, Fig. 8), which represents simultaneous N-H $\cdots\pi$, C-H \cdots F and C-H \cdots O interactions, has a slightly lower interaction energy.

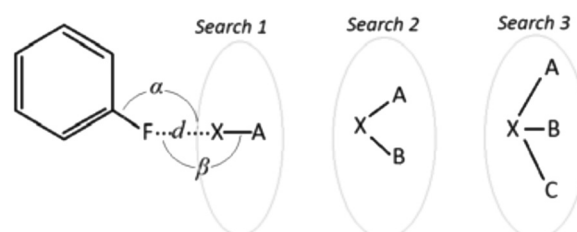
The planar geometry of these two molecules, where N-H \cdots F and C-H \cdots O interactions simultaneously occur, has also a significantly higher interaction energy ($-5.67 \text{ kcal mol}^{-1}$, Fig. 8). Despite the fact that the most stable interaction of two fluorobenzenes (PhF:PhF-1) is equal to the strength of the most stable interaction between cyclohexane and fluorobenzene (PhF:ChH), in the crystal structure of **2** the cyclohexyl ring builds the largest number of interactions with the phenyl ring. To understand why this happens, it has been necessary to consider the structure of the studied compound. Namely, the hydantoin ring, as the central part of the compound, forms a pair of N-H \cdots O hydrogen bonds with another hydantoin ring. The approach of the cyclohexyl ring from the upper side of the hydantoin ring is sterically hindered by the cyclohexyl and phenyl rings, thus making the cyclohexyl ring accessible only for the weak C-H \cdots O interactions. The interaction with another cyclohexane ring (in the most favorable orientation is $-3.02 \text{ kcal mol}^{-1}$, ChH:ChH-1 dimer, Fig. 7) is slightly weaker than the interaction with the fluorobenzene ring. In addition, the cyclohexane ring is more voluminous than the fluorobenzene ring, so a greater number of simultaneous interactions of the cyclohexane ring with this ring is possible. When it comes to ring-overlapping interactions, the cyclohexane ring can build C-H \cdots F interactions with the fluorobenzene ring, which is energetically more favourable than the hydrophobic one. Precisely, these interactions (C-H \cdots F interactions) are the

reason for a larger number of contacts of the cyclohexyl ring with the phenyl ring in the crystal structure of **2**. Seven contacts between cyclohexane and fluorobenzene have been identified in the crystal structure of **2**, whereby three of them are C-H \cdots F interactions. The reason why the interactions of the aromatic and hydantoin rings are less abundant than the interactions involving the cyclohexane ring, despite being multiply stronger, has already been partially indicated. In two most stable geometries of the PhF:Hyd dimer, the aromatic ring is located above the hydantoin ring and this approach is sterically hindered. In the planar geometry (PhF:Hyd-3 dimer), the interaction involves the hydantoin N-H and C=O groups. In the crystal structure, however, these groups are engaged in hydrogen bonding with other hydantoin rings and this type of interaction is significantly stronger than the interaction in the planar geometry.

A CSD study

Replacement of the hydrogen atom with the fluorine atom has led to changes in the crystal packing as a consequence of differences in the strengths and types of interactions that occur between the phenyl ring and other two rings. This is also indicated by the data on the nature of atoms located at a distance less than 4 \AA from the fluorine atom in **2**, *i.e.*, from the hydrogen atom in the same position in **1**.

Seven hydrogen atoms and one oxygen atom are in contact with the fluorine atom in the crystal packing of **2**. Six hydrogen atoms originate from four neighboring cyclohexane rings, one hydrogen atom from the neighboring aryl group, while the oxygen atom belong to the carbonyl group of the hydantoin ring. In the case of **1**, there are six hydrogen atoms from three neighboring cyclohexane rings and one oxygen atom from the bridging carbonyl group. Replacement of the hydrogen atom with the fluorine atom has led not only to an increase in the number of the contact rings, but also to a transition from hydrophobic to C-H \cdots F interactions. It is interesting that the fluorine atom interacts even with the oxygen atom through the C=O \cdots F interaction.



Scheme 1 The model systems and geometric parameter used for searching of the CSD. The V1/P parameter is the angle between the vector V1 and the plane P of the aromatic ring. In search 1, the vector V1 is the (AX) \rightarrow vector, while, in search 2, the vector V1 represents the $\overline{\Omega_{AB}X}$ vector, where Ω_{AB} is the center of mass of the A and B atoms. Concerning search 3, it is the $\overline{\Omega_{ABC}X}$ vector where Ω_{ABC} represents the center of mass of the A, B and C atoms.

Table 2 Results of the CSD search for interaction of the F atoms bonded to the aromatic ring

	Search 1	Search 2	Search 3
Number of structures	17 906	2745	196
Number of interactions	472 648	4447	258
Percentage of cetrain atoms in position X	70.2% H 27.1% F	47% O 21% S 20% N	18% C

To obtain a more extensive insight into the interactions involving the fluorine atom, a statistical analysis of the data obtained by the CSD search has been performed (Scheme 1). Namely, 17 906 structures with 472 648 F...X interactions have been identified in search 1, 2745 structures with 4447 F...X interactions have been found in search 2 and 196 structures with 258 F...X interactions have been retrieved in search 3 (Table 2). The statistical analysis of interactions has shown that a hydrogen atom (70.2%) and a fluorine atom (27.1%) have mainly been found in position X in the structures obtained in search 1.

The other elements are significantly less represented (1.2% O, 0.8% Cl, 0.2% Br and 0.2% I). Search 2 has revealed that an oxygen atom is in position X in 47% of the interactions, while a sulphur atom and a nitrogen atom are in 21 and 20% of the interactions, respectively. The smallest set of the structures has been obtained in search 3 and these structures have a sulphur, nitrogen, carbon, oxygen or phosphorus atom in position X, with the abundance of carbon being 18%, while other atoms have an abundance of about 10%.

A similar trend has been obtained with the boundary distance of 3.5 Å, although this search includes the fluorine atom bound not only to the phenyl ring but also to other groups and rings.⁹ Therefore, it can be concluded that reduction of a boundary criterion of the distance d leads to an increase in the number of hydrogen atoms (X-H...F interactions), while the abundance of other atoms decreases. The F...F interactions (127 972 interactions) are the second most common in the crystal structures (after X-H...F interactions). Moreover, the F...F interactions are multiply larger in number than interactions involving other halogen elements with the ability to form the σ -hole (Cl, Br, and I), which further results in the possibility of the electrostatic

interactions between the σ -hole and the free electron pairs of the fluorine atom.

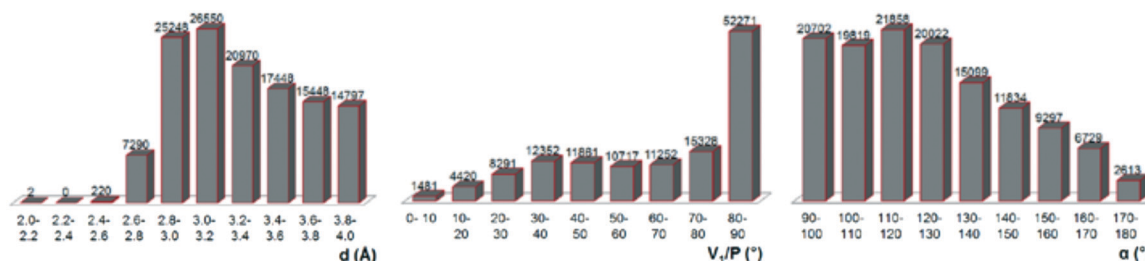
The statistical analysis of the geometrical parameters for the F...F interactions (Fig. 9) has shown that the distances of the interacting fragments are in the range from 2.0 to 4.0 Å, with the maximum distribution between 2.8 and 3.2 Å. It is important to emphasize that the number of interactions decreases when the distance d is greater than 3.2 Å, but not drastically. The relative orientation of the interacting fragments is mostly parallel (the V1/P angle close to 90°).

The distribution of the α angles (C-F...X) indicates that the number of the structures decreases when this angle is greater than 130°. A similar distribution has been found for the α angles in the range from 90° to 130°, thus indicating that the interacting fluorine atom is not above the aromatic ring nor the fluorine atom, but it is located outside the aromatic group.

F...F interactions in the crystal structure of 2

In the crystal packing of 2, there are no F...F interactions which fulfil the above defined geometrical criteria. However, an interaction between the fluorine atoms at the distance d larger than the limiting one (4.26 Å) has been identified, the energy of which is -0.17 kcal mol⁻¹. Although energetically non-significant, this interaction might have a supramolecular importance. Interaction energy of the motif, wherein the *para*-substituent in 2 has been replaced by the hydrogen atom, is only -0.02 kcal mol⁻¹ (Fig. S7†). As the carbonyl group (part of the *para*-substituent) exerts electron-withdrawing effects, reduced negative potential of the F atom can be expected. This might be a reason of a higher interaction energy in the case of 2. Namely, this reduction in the negative potential led to lower repulsion which is a significant component of the interaction energy between two electronegative atoms.

To determine the value of the distance d which is acceptable as the optimal distance, we have performed the calculations on the model system presented in Fig. 10 in a way that the relative orientation of the molecules has been kept constant and the distance d has been systematically changed. Namely, the values of the distance d of 4.26, 3.50, 3.25 and 3.0 Å have been considered, thus resulting in the interaction energies of -0.17 , -0.39 , -0.46 and -0.43 kcal mol⁻¹, respectively. It can be concluded that the shortening

**Fig. 9** Distributions of the geometrical parameters for description of the F...F interactions in the crystal structures extracted from the CSD.

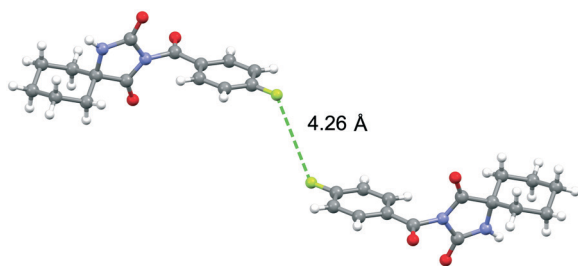


Fig. 10 Model system extracted from the crystal packing of **2** formed through the F...F interaction with interaction energy of $-0.17 \text{ kcal mol}^{-1}$.

the distance results in the interaction strengthening with a shallow minimum of interaction energies from -0.40 to $-0.50 \text{ kcal mol}^{-1}$ corresponding to the range from 3.0 to 3.5 \AA . Anyway, the F...F interactions are very weak in this case, although a slight increase in the interaction energy can be identified. For comparison, the energy of the strongest F...F interaction between two molecules of fluoromethane is $-1.44 \text{ kcal mol}^{-1}$.⁹ To analyze the supramolecular significance of the F...F interaction, its cooperative effect as well as the effect of simultaneous interactions should be taken into account. The cooperative effect can be rationalized as the effect of a species from the environment on the F...F interaction. On the other side, the effect of simultaneous interactions is reflected on the strength of interactions which a species from the environment forms with both F atoms.

Map of electrostatic potential (MEP)

Beside the dispersion, the electrostatic component of energy often makes the greatest contribution to the total interaction energy.⁹ To obtain an insight into the distribution of potentials, *i.e.*, the distribution of electron density, and, hence, to explain why some fragments of the interacting species are attracted to each other, electrostatic maps of potentials have been analyzed. These maps are also very

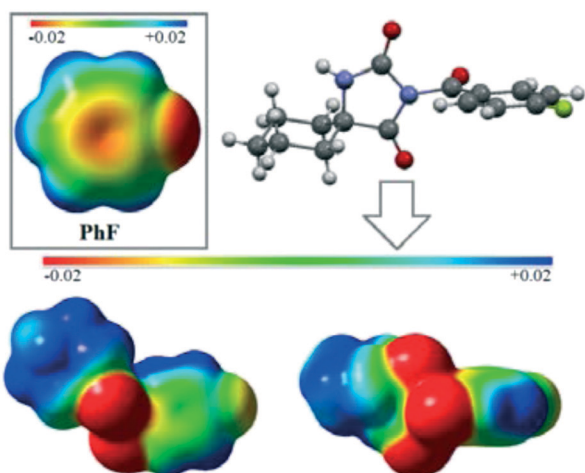


Fig. 11 Maps of electrostatic potential of fluorobenzene and **2**.

useful in examining the cooperative effect and the effects of simultaneous interactions, which will be discussed below.

In fluorobenzene, the part with the most negative potential is located on the fluorine atom (Fig. 11). Also, the π -system has a negative potential, although smaller than that on the F atom. The negative potential increases as moving from the edge of the ring towards the centre of the π -system. The positive potential is located on the hydrogen atoms. By comparing this map with the potential map of **2** (Fig. 11), it can be noted that substitution in the *para* position relative to the fluorine atom has led to colour changes in the maps. Namely, the carbonyl group in the *para* position has an electron-withdrawing character, which further has led to a shift of the electron density from the ring to the substituent. This shift causes a decrease of the negative potential above the π -system and an increase of the positive potential on the hydrogen atoms. There is also a decrease of the negative potential on the fluorine atom. From the supramolecular point of view, introduction of the carbonyl group as a substituent should lead to a decrease in the strength of interactions wherein the aromatic fragment has the accepting role and an increase in the strength of interactions wherein this ring has the hydrogen bond donating role. The most negative part in **2** is located on the carbonyl oxygen atoms, while the cyclohexyl ring has a positive potential at its entire surface.

The formation of the $\text{C}(\text{sp}^3)\text{-F}\cdots\text{F}\text{-C}(\text{sp}^3)$ interactions results in an increase in the electron density, *i.e.*, the negative potential in the contact region.¹³ To examine whether the $\text{C}(\text{sp}^2)\text{-F}\cdots\text{F}\text{-C}(\text{sp}^2)$ interactions cause the changes in the electron density and the electrostatic potential, MEPs of the motif extracted from the crystal structure of **2** have been calculated for a set of the intermolecular distances (3.0 , 3.5 and 4.26 \AA , Fig. 12). Based on these maps, it can be

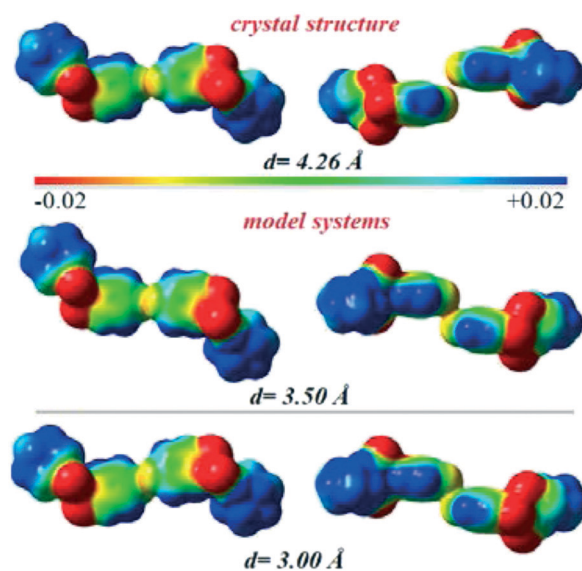


Fig. 12 Maps of electrostatic potential of the motif extracted from the crystal structure of **2** for a set of distances between the molecules.

concluded that there is no significant change in the blue colour above the C–H groups of the benzene ring, which indicates a positive potential and, therefore, no significant changes of the donating abilities of this fragment should be expected. By analysing the π -system from the outer side of the model system, it can be noticed that, with a decrease of the distance d , there is a decrease of the area with green colour (neutral potential) and a slight increase of the blue region (slightly positive potential). The sides of the π -system facing the F \cdots F interaction do not have any significant change in potential with a distance change. The formation of F \cdots F interaction leads to an increase in the intensity of the yellow colour on the fluorine atoms, in comparison to the fluorine atom in monomers, which indicates an increase of the negative potential in the region of the F \cdots F interaction.

Effects of simultaneous interactions

By analysing electrostatic potential maps, it can be concluded that the F \cdots F interactions lead to formation of a new acceptor region with a larger surface area and a slightly higher negative potential in comparison to the individual fluorine atoms. All these changes result in formation of more simultaneous interactions with the surrounding species, thus allowing the denser crystal packing.

In the crystal structure of **2**, the F \cdots F region simultaneously interacts with four surrounding molecules, which, due to symmetry, can be associated with two interaction types. Regarding the first type, a molecule from the surrounding (species A, Fig. 13) formed a C–H \cdots F interaction ($\Delta E = -1.71$ kcal mol $^{-1}$) with the first fluorine atom from the F \cdots F region (from the F1 species, corresponding to the motif F5) and a C–H \cdots F interaction ($\Delta E = -3.12$ kcal mol $^{-1}$) with the molecule bearing the second

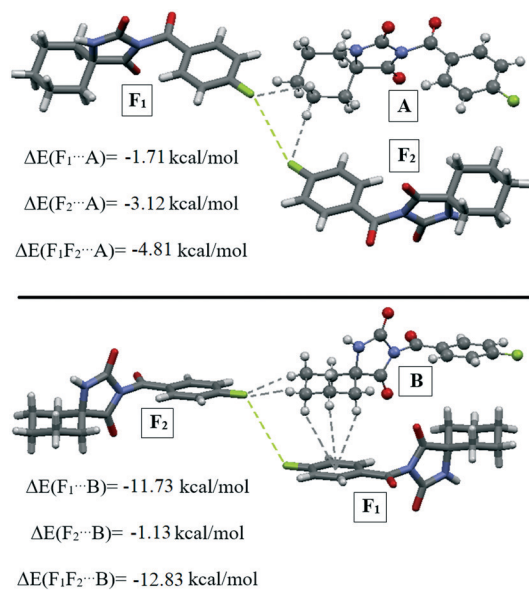


Fig. 13 Trimeric systems, extracted from the crystal packing of **2**, used for investigation of effect of simultaneous interactions.

fluorine atom involved in the F \cdots F region (from the F2 species, corresponding to motif the F8). However, the total interaction energy of the interactions that this molecule (species A) simultaneously builds with both molecules of the F \cdots F region ($\Delta E = -4.81$ kcal mol $^{-1}$) is similar to the sum of the energies of the individual C–H \cdots F interactions ($\Delta E = -4.83$ kcal mol $^{-1}$). Even when the energy of F \cdots F (F1 \cdots F2 species) interaction of the observed motif ($\Delta E = -0.17$ kcal mol $^{-1}$) is added to the total interaction energy, it cannot be claimed that the formation of the F \cdots F interaction leads to a substantial increase in energy in this case, *i.e.*, there is no pronounced effect originating from the simultaneous interactions. In the second case, a molecule from the surrounding (species B, Fig. 11) forms stronger interactions with both molecules involved in formation of the F \cdots F region ($\Delta E = -12.83$ kcal mol $^{-1}$) in comparison to interactions with the individual molecules (formation of trifurcated C–H \cdots π interaction with $\Delta E = -11.73$ kcal mol $^{-1}$ and bifurcated C–H \cdots F interaction with $\Delta E = -1.13$ kcal mol $^{-1}$, corresponding to the motifs F5 and F2 motifs). In this system, there is no effect of simultaneous interactions, because the total interaction energy is similar to the sum of the individual energies (the sum of the ΔE is -12.86 kcal mol $^{-1}$).

Cooperative effect of the F \cdots F interaction

To determine whether the change in the strength of the F \cdots F interaction cooperatively affects other interactions wherein only one of the molecules involved in the F \cdots F interaction participates, calculations have been performed on model trimeric systems extracted from the crystal structure of **2**

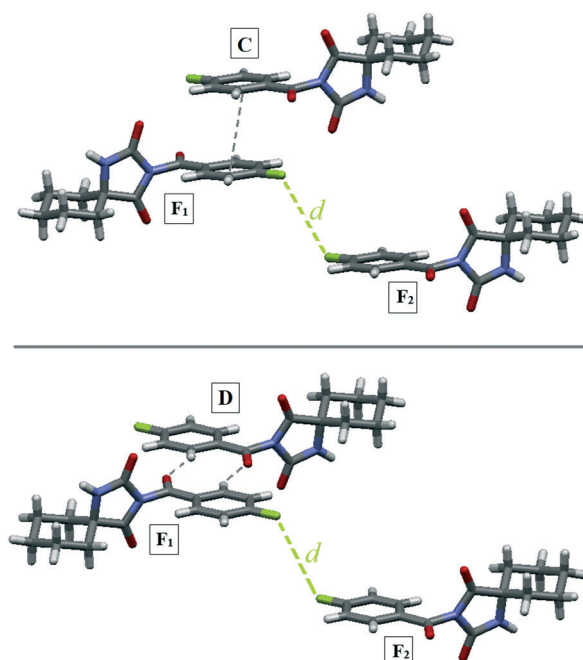


Fig. 14 Trimeric systems modelled for investigation of the cooperative effect resulting from formation of the F \cdots F interaction.

Table 3 Results of calculations performed on the dimeric and trimeric systems modelled to examine the cooperative effect resulting from formation of the F...F interactions (interaction energy, ΔE is in kcal mol⁻¹ and the distances d is in Å)

Crystal structure	Model systems			
	$d = 3.00$	$d = 3.25$	$d = 3.50$	$d = 4.26$
$\Delta E(F_1/F_2)$	$\Delta E(F_1/F_2)$			
-0.17	-0.43	-0.46	-0.39	-0.17
$\Delta E(C/F_1)$	$\Delta E(C/F_1F_2)$			
-9.03	-9.22	-9.16	-9.10	-9.00
$\Delta E(D/F_1)$	$\Delta E(D/F_1F_2)$			
-5.04	-4.92	-4.92	-4.92	-4.93

(Fig. 14). In the first model system, a molecule from the surrounding (species C) builds a stacking interaction with one of the molecules involved in the F...F interaction (with the species F1, corresponding to the motif F3), with the interaction energy of 9.03 kcal mol⁻¹. When the third molecule (species F2 involved in the F...F interaction) from the crystal packing of 2 has been taken into account, this stacking interaction slightly strengthens. When examining this effect, the changes in strength of the stacking interaction between the C and F1 species has been monitored by changing the length of the F...F interaction. The highest interaction energy of -9.22 kcal mol⁻¹ corresponds to the distance d of 3.0 Å. The strengthening of the stacking interaction as a result of the F...F interaction (-0.19 kcal mol⁻¹) and the energy of F...F interaction within the motif (-0.43 kcal mol⁻¹) give the total cooperative effect of -0.62 kcal mol⁻¹.

In the second model system, a molecule from the surrounding (species D) interacts with one of the molecules involved in the F...F interaction (species F1) through a pair of the C-H...O interactions (corresponding to the motif F9). The interaction (D/F1) energy of -5.04 kcal mol⁻¹ is slightly higher than that of the trimeric system (D/F1F2 system) with the second molecule (species F2) involved in the F...F interaction. In this case, interaction energy is -4.93 kcal mol⁻¹. A decrease in the distance d of F...F interaction does not affect the strength of the C-H...O interactions (Table 3). The highest cooperative effect of -0.34 kcal mol⁻¹ corresponds to the distance d of 3.25 Å (the energy of the F...F interaction of -0.46 kcal mol⁻¹ + energy reduction of a pair of the C-H...O interactions due to establishment of the F...F interaction of 0.12 kcal mol⁻¹).

Having in mind both model systems, it can be concluded that the strengthening of the F...F interactions has a greater impact on the strength of the stacking interaction than on the C-H...O interaction (Table 3). In other words, the strengthening of the F...F interactions causes greater changes of the π -system than in the donating abilities of the C(sp²)-H groups.

Conclusion

The presented crystallographic and quantum chemical study is focused on effects of fluorination of the phenyl ring linked

to the spirohydantoin moiety by a carbonyl bridge. The greatest contribution to the stabilization of the crystal packing comes from the hydantoin moieties which build a pair of N-H...O hydrogen bonds with interaction energy of around -21 kcal mol⁻¹. Additionally, these moieties are connected to other rings by means of C-H...O interactions. In the crystal packing of 1, the phenyl ring has the highest affinity towards the cyclohexyl ring and established five interactions with it. When the fluorine atom is introduced into the phenyl ring, this affinity increases (seven interactions) due to formation of the C-H...F interactions. Although fluorination of the phenyl ring results in strengthening of the interactions between these two rings, only two interactions (stacking interactions and PILO) between the aromatic rings can be identified in both crystal structures. A reason is strengthening and interaction between the cyclohexyl and fluorinated phenyl ring.

The analysis of the contact atoms in the neighbourhood of the fluorine atom in the crystal packing of 2 has shown that the hydrogen atoms are the most frequent as a result of the C-H...F interactions. Besides, the carbonyl oxygen atom has also been found, thus resulting in formation of the F...O interaction. However, the results of an analysis of the contact atoms at distances shorter than 4 Å to the fluorine atoms in the crystal structures deposited in the CSD is only in a partial agreement with that observed in the crystal packing of 2. Namely, the fluorine atoms establish interactions with the hydrogen atoms most often, then come the F...F interactions, while interactions with the oxygen atoms are at the third place. Although the fluorine atom exerts a higher affinity toward F...F interactions, formation of F...O interaction in the crystal packing of 2 is supported by simultaneous stacking interaction between the phenyl rings. In this case, the F...F interaction at a large distance ($d = 4.26$ Å) has been recognized. In this dimeric motif, there are no simultaneous interactions between the other structural fragments of 2, thus resulting in the low interaction energy (-0.17 kcal mol⁻¹). The DFT calculations indicate that shortening of the distance d does not lead to significant changes in the interaction energies being, in the best case, up to -0.5 kcal mol⁻¹. Despite the unfavourable geometry, the symmetry elements of this motif indicate its supramolecular significance. The electrostatic potential maps show that formation of the F...F interaction causes an increase in the negative potential on the interacting fluorine atoms, a decrease in the negative potential above the π -system as well as an increase in the positive potential surface above the hydrogen atoms of the phenyl ring. The calculations on the trimeric model systems demonstrate that these changes in the potentials are followed by the cooperative effect. Namely, formation of the F...F interactions can lead to strengthening of interaction of one of the fluorine atoms with a molecule from the environment which does not simultaneously interact with both of them. It is evident that formation of the F...F interaction is followed by strengthening of stacking interactions, while C-H...O interactions weaken. When the third molecule interacts with

both fluorine atoms simultaneously, the calculations show that the effect of strengthening of individual interactions due to formation of F...F interactions is absent.

Although the effect of simultaneous interactions has not been observed, formation of F...F interactions is favoured for a reason which still involves the ability of the system to build simultaneous interactions. Namely, through formation of F...F interactions a region of the increased electron density with the surface greater than the one of the individual fluorine atoms emerges. Therefore, formation of F...F interactions leads to an increase in the surface with the accepting ability, which, not only has the greater electron density in comparison with the individual fluorine atoms, but also enables establishment of a greater number of simultaneous interactions with the surrounding species. A greater number of species in the environment of F...F interaction further causes an increase in number of interactions with the F...F region, as well as an increase in the number of their interactions with other structural fragments of the molecules forming F...F interaction. Finally, this increase in the number of interactions and, hence, the higher interaction energy result in a denser crystal packing. An analogous phenomenon should be expected for F...O interactions, thus explaining their abundance contrary to the chemical intuition which does not support frequent formation of interactions between two electronegative atoms.

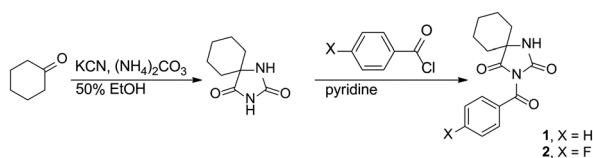
Experimental

Synthetic procedure

The investigated compounds **1** and **2** were obtained following the synthetic protocol shown in Scheme 2. Cyclohexane-5-spirohydantoin was synthesized by the method of Bucherer and Lieb²⁴ and it was further acylated using a modified procedure described previously.²⁵

The investigated compounds were characterized by melting point determination, FT-IR, ¹H and ¹³C NMR spectroscopy and elemental analysis. The melting point was measured on an electrothermal melting point apparatus without correction. The FT-IR spectra were measured using Bomem MB spectrophotometer and ¹H and ¹³C NMR spectra were recorded on a Bruker AC 250 spectrometer. Elemental analyses were carried out using microanalyzer Elemental Vario EL III.

General procedure for synthesis of the investigated compounds. Cyclohexane-5-spirohydantoin (0.84 g, 0.005 mol) was suspended in dried pyridine (5 ml) and the corresponding acyl chloride (0.005 mol) was added dropwise



Scheme 2 Synthesis of compounds **1** and **2**.

to the mixture and stirred at room temperature overnight. After the completion of the reaction, pyridine was evaporated under vacuum and the residue was dissolved in ethyl acetate. The solution was washed with 5% NaOH and water and dried over anhydrous MgSO₄. The residual solvent was removed and the crude product was purified by recrystallization from ethyl alcohol.

3-Benzoyl-1,3-diazaspiro[4.5]decane-2,4-dione (1). Yield: 0.41 g (30%); m.p.: 163–166 °C; IR (ATR): $\nu = 3226, 3112, 2930, 2861, 1791, 1744, 1692, 1448, 1378, 1345, 1295, 1259, 1135, 1101, 1016, 996, 926, 843, 810, 759, 691, 634 \text{ cm}^{-1}$; ¹H NMR (400 MHz, DMSO-*d*₆): $\delta = 9.21$ (s, 1H, NH), 7.85 (d, 2H, *J* = 7.6 Hz, -C₆H₅), 7.73 (t, 1H, *J* = 7.6 Hz, -C₆H₅), 7.56 (t, 2H, *J* = 7.6 Hz, -C₆H₅), 1.77–1.55 (m, 9H, cycC₆H₁₀), 1.36–1.23 (m, 1H, cycC₆H₁₀) ppm; ¹³C NMR (100 MHz, DMSO-*d*₆): $\delta = 175.3, 167.9, 152.6, 135.1, 132.7, 130.6, 129.3, 62.0, 33.8, 24.7, 21.2$ ppm; elemental analysis calcd (%) for C₁₅H₁₆N₂O₃: C 66.15, H 5.92, N 10.29; found: C 66.18, H 5.83 N, 10.35.

3-(4-Fluorobenzoyl)-1,3-diazaspiro[4.5]decane-2,4-dione (2). Yield: 0.68 g; (47%); m.p.: 198–201 °C; IR(ATR): 3187, 3106, 2927, 2866, 1780, 1708, 1594, 1504, 1468, 1453, 1433, 1384, 1346, 1290, 1274, 1257, 1219, 1154, 1134, 1101, 1007, 978, 928, 826, 801, 760, 726, 713, 679, 614 cm⁻¹; ¹H NMR (400 MHz, DMSO-*d*₆): $\delta = 9.21$ (s, 1H, NH), 7.96 (q, 2H, *J* = 4.8 Hz, -C₆H₄-), 7.39 (t, 2H, *J* = 8.8 Hz, -C₆H₄-), 1.81–1.52 (m, 9H, cycC₆H₁₀), 1.34–1.27 (m, 1H, cycC₆H₁₀) ppm; ¹³C NMR (100 MHz, DMSO-*d*₆): $\delta = 175.2, 166.3$ (d, *J* = 254 Hz), 166.2, 152.5, 133.8 (d, *J* = 9.9 Hz), 129.4 (d, *J* = 2.6 Hz), 116.5 (d, *J* = 23 Hz), 62.0, 33.7, 24.7, 21.1 ppm; elemental analysis calcd (%) for C₁₅H₁₅FN₂O₃: C 62.06, H 5.21, N 9.65; found: C 61.97; H 5.18; N 9.56.

Crystal structure determination

Single crystals suitable for an X-ray structure determination were obtained by slow evaporation of acetonitrile solutions at room temperature. Single-crystal X-ray diffraction data were collected at room temperature on an Oxford Gemini S diffractometer equipped with CCD detector using monochromatized MoK α radiation ($\lambda = 0.71073 \text{ \AA}$). Intensities were corrected for absorption using the multiscan method. The structures were solved by direct methods using SIR2014 (ref. 26) and refined on *F*² by full-matrix least-squares using the programs SHELXL-2018/3 (ref. 27) and WinGX.²⁸ All non-hydrogen atoms were refined anisotropically. The positions of the H atoms connected to the C and N atoms were calculated on geometric criteria and refined by the riding model with $U_{\text{iso}} = 1.2U_{\text{eq}}(\text{C, N})$. Selected crystal data and refinement results for **1** and **2** are listed in Table 1. CCDC 2045907 and 2045908 for **1** and **2**, respectively contain the ESI[†] crystallographic data for this paper.

Quantum-chemical calculations

To understand the crystal packing of **1** and **2**, the quantum-chemical calculations at TPSSH-D3/def2TZVP level were performed in the Gaussian 09 software.²⁹ All model systems

were extracted from the crystal structures and used to estimate the strength of non-covalent interactions. The atomic coordinates are maintained from the solved crystal structures, except for the positions of the H atoms. The positions of the H atoms are determined by optimization of model systems, with frozen non-hydrogen atoms (with this approach, the accuracy of the H position was achieved). The interaction energies (ΔE) were computed as the difference in energy between the dimer and the sum of the optimized energies of the isolated monomers, corrected for basis set superposition error (BSSE) by the counterpoise method.³⁰

The Hirshfeld surface analysis and associated 2D fingerprint plots were carried out using the CrystalExplorer 17.5.³¹ The d_{norm} surface was mapped with the color scale in the range -0.5614 au (red) to 1.2927 au (blue). The 2D fingerprint plots (d_i vs. d_e) were displayed using the standard range. Calculations were done at accurate B3LYP/6-31g(d,p) level of theory using Gaussian 09 program package.

The lattice energies of the compounds were calculated at MP2/6-31(d,p) and B3LYP/6-31(d,p) level of theory using Gaussian 09 program package and PIXELC module19 from CLP computer program package (version 12.5.2014).²⁰

Statistical analysis of the crystal structures from the CSD

The search for the crystal structures from the Cambridge Structural Database (CSD, version 5.36)⁵ was based on the model system shown in Scheme 1. Using the program ConQuest 1.10,³² all structures containing F \cdots X interaction with the d distance less than 4.0 \AA were extracted. In addition, the structures were considered as a hit if the angles $\alpha(\text{C-F}\cdots\text{X})$ and $\beta(\text{F}\cdots\text{X-A}, \text{F}\cdots\text{X-B}, \text{and } \text{F}\cdots\text{X-C})$ were greater than 90° in order to avoid structures where F \cdots X interaction was a consequence of the F \cdots A, F \cdots B or F \cdots C interactions.

Conflicts of interest

There are no conflicts to declare.

Acknowledgements

This work was supported by the Ministry of Education, Science and Technological Development of the Republic of Serbia (Contract No. 451-03-9/2021-14/200135; 451-03-9/2021-14/200287, 451-03-9/2021-14/200026 and OI 171035).

Notes and references

- (a) H. J. Böhm, D. Banner, S. Bendels, M. Kansy, B. Kuhn, K. Müller, U. Obst-Sander and M. Stahl, *ChemBioChem*, 2004, **5**, 637; (b) N. A. Meanwell, K. J. Eastman and E. P. Gillis, Tactical applications of fluorine in drug design and development, in *Fluorine in heterocyclic chemistry*, ed. V. Nenajdenko, Springer International, Cham, 2014, vol. 1, pp. 1–54; (c) E. P. Gillis, K. J. Eastman, M. D. Hill, D. J. Donnelly and N. A. Meanwell, *J. Med. Chem.*, 2015, **58**, 8315.
- (a) K. Reichenbacher, H. I. Süß and J. Hulliger, *Chem. Soc. Rev.*, 2005, **34**, 22; (b) D. Chopra and T. N. Guru Row, *CrystEngComm*, 2011, **13**, 2175; (c) P. Panini and D. Chopra, Understanding of noncovalent interactions involving organic fluorine, in *Hydrogen bonded supramolecular structures*, ed. Z. Li and L. Wu, Springer-Verlag, Berlin Heidelberg, 2015, pp. 37–67.
- J. D. Dunitz and R. Taylor, *Chem. – Eur. J.*, 1997, **3**, 89.
- V. R. Thalladi, H. C. Weiss, D. Bläser, R. Boese, A. Nangia and G. R. Desiraju, *J. Am. Chem. Soc.*, 1998, **120**, 8702.
- C. R. Groom, I. J. Bruno, M. P. Lightfoot and S. C. Ward, *Acta Crystallogr., Sect. B: Struct. Sci., Cryst. Eng. Mater.*, 2016, **72**, 171.
- J. A. K. Howard, V. J. Hoy, D. O'Hagan and G. T. Smith, *Tetrahedron*, 1996, **52**, 12613.
- J. R. Loader, S. Libri, A. J. H. M. Meijer, R. N. Perutz and L. Brammer, *CrystEngComm*, 2014, **16**, 9711.
- A. R. Choudhury and T. N. Guru Row, *Cryst. Growth Des.*, 2004, **4**, 47.
- G. V. Janjić, S. T. Jelić, N. P. Trišović, D. M. Popović, I. S. Dorđević and M. K. Milčić, *Cryst. Growth Des.*, 2020, **20**, 2943.
- N. Ramasubbu, R. Parthasarathy and P. Murray-Rust, *J. Am. Chem. Soc.*, 1986, **108**, 4308.
- M. Barcelo-Oliver, C. Estarellas, A. Garcia-Raso, A. Terron, A. Frontera, D. Quiñero, I. Mata, E. Molins and P. M. Deya, *CrystEngComm*, 2010, **12**, 3758.
- V. A. Karnoukhova, I. V. Fedyanin and K. A. Lyssenko, *Struct. Chem.*, 2016, **27**, 17.
- A. Bauzá and A. Frontera, *Phys. Chem. Chem. Phys.*, 2016, **18**, 20381.
- R. J. Baker, P. E. Colavita, D. M. Murphy, J. A. Platts and J. D. Wallis, *J. Phys. Chem. A*, 2012, **116**, 1435.
- (a) L. Konnerth, F. Lamaty, J. Martinez and E. Colacino, *Chem. Rev.*, 2017, **117**, 13757; (b) M. Gregoriou, M. E. M. Noble, K. A. Watson, E. F. Garman, L. N. Johnson, T. M. Krulle, C. De La Fuetene, G. W. J. Fleet and N. G. Oikonomakos, *Protein Sci.*, 1998, **7**, 915.
- P. Vachal, S. Miao, J. M. Pierce, D. Guiadeen, V. J. Colandrea, M. J. Wyratt, S. P. Salowe, L. M. Sonatore, J. A. Milligan, R. Hajdu, A. Gollapudi, C. A. Keohane, R. B. Lingham, S. M. Mandala, J. A. DeMartino, X. Tong, M. Wolff, D. Steinhuebel, G. R. Kieczkowski, F. J. Fleitz, K. Chapman, J. Athanasopoulos, G. Adam, C. D. Akyuz, D. K. Jena, J. W. Lusen, J. Meng, B. D. Stein, L. Xia, E. C. Sherer and J. J. Hale, *J. Med. Chem.*, 2012, **55**, 2945.
- S. H. Watterson, Z. Xiao, D. S. Dodd, D. R. Tortolani, W. Vaccaro, D. Potin, M. Launay, D. K. Stetsko, S. Skala, P. M. Davis, D. Lee, X. Yang, K. W. McIntyre, P. Balimane, K. Patel, Z. Yang, P. Marathe, P. Kadiyala, A. J. Tebben, S. Sheriff, C. Y. Chang, T. Ziemba, H. Zhang, B. C. Chen, A. J. DelMonte, N. Aranibar, M. McKinnon, J. C. Barrish, S. J. Suchard and T. G. Murali Dhar, *J. Med. Chem.*, 2010, **53**, 3814.
- (a) S. Graus, D. Casabona, S. Uriel, C. Cativiela and J. L. Serrano, *CrystEngComm*, 2010, **12**, 3132; (b) P. T. Todorov,

- R. N. Petrova, E. D. Naydenova and B. L. Shivachev, *Cent. Eur. J. Chem.*, 2009, **7**, 14; (c) A. Lazić, N. Trišović, L. Radovanović, J. Rogan, D. Poleti, Ž. Vitnik, V. Vitnik and G. Ušćumlić, *CrystEngComm*, 2017, **19**, 469; (d) A. M. Lazić, L. D. Radovanović, B. Đ. Božić, B. Đ. Božić Nedeljković, V. D. Vitnik, Ž. J. Vitnik, J. R. Rogan, N. V. Valentić, G. S. Ušćumlić and N. P. Trišović, *J. Mol. Struct.*, 2019, **1180**, 48.
- 19 (a) M. A. Spackman, J. J. McKinnon and D. Jayatilaka, *CrystEngComm*, 2008, **10**, 377; (b) M. A. Spackman and D. Jayatilaka, *CrystEngComm*, 2009, **11**, 19.
- 20 (a) A. Gavezzotti, *Molecular Aggregation*, Oxford University Press, Oxford, 2005, ch. 12; (b) A. Gavezzotti, *J. Phys. Chem. B*, 2003, **107**, 2344; (c) A. Gavezzotti, *Mol. Phys.*, 2008, **106**, 1473.
- 21 C. F. Mackenzie, P. R. Spackman, D. Jayatilaka and M. A. Spackman, *IUCrJ*, 2017, **4**, 575.
- 22 D. B. Ninković, G. V. Janjić, D. Ž. Veljković, D. N. Sredojević and S. D. Zarić, *ChemPhysChem*, 2011, **12**, 3511.
- 23 D. Ž. Veljković, G. V. Janjić and S. D. Zarić, *CrystEngComm*, 2011, **13**, 5005.
- 24 (a) H. T. Bucherer and V. A. Lieb, *J. Prakt. Chem.*, 1934, **141**, 5; (b) I. A. Rivero, E. A. Reynoso and A. Ochoa-Teran, *ARKIVOC*, 2011, 260.
- 25 R. Yousefi, D. C. Whitehead, J. M. Mueller, R. J. Staples and B. Borhan, *Org. Lett.*, 2011, **13**, 608.
- 26 M. C. Burla, R. Caliandro, B. Carrozzini, G. L. Casciarano, C. Cuocci, C. Giacovazzo, M. Mallamo and A. Mazzone, *J. Appl. Crystallogr.*, 2015, **48**, 306.
- 27 G. M. Sheldrick, *Acta Crystallogr., Sect. C: Struct. Chem.*, 2015, **71**, 3.
- 28 L. J. Farrugia, *J. Appl. Crystallogr.*, 2012, **45**, 849.
- 29 M. J. Frisch, G. W. Trucks, H. B. Schlegel, G. E. Scuseria, M. A. Robb, J. R. Cheeseman, G. Scalmani, V. Barone, B. Mennucci, G. A. Petersson, H. Nakatsuji, M. Caricato, X. Li, H. P. Hratchian, A. F. Izmaylov, J. Bloino, G. Zheng, J. L. Sonnenberg, M. Hada, M. Ehara, K. Toyota, R. Fukuda, J. Hasegawa, M. Ishida, T. Nakajima, Y. Honda, O. Kitao, H. Nakai, T. Vreven, J. A. Montgomery Jr., J. E. Peralta, F. Ogliaro, M. Bearpark, J. J. Heyd, E. Brothers, K. N. Kudin, V. N. Staroverov, R. Kobayashi, J. Normand, K. Raghavachari, A. Rendell, J. C. Burant, S. S. Iyengar, J. Tomasi, M. Cossi, N. Rega, N. J. Millam, M. Klene, E. J. Knox, J. B. Cross, V. Bakken, C. Adamo, J. Jaramillo, R. Gomperts, R. E. Stratmann, O. Yazyev, A. J. Austin, R. Cammi, C. Pomelli, J. W. Ochterski, R. L. Martin, K. Morokuma, V. G. Zakrzewski, G. A. Voth, P. Salvador, J. J. Dannenberg, S. Dapprich, A. D. Daniels, Ö. Farkas, J. B. Foresman, J. V. Ortiz, J. Cioslowski and D. J. Fox, *Gaussian09*, Gaussian, Inc., Wallingford, 2009.
- 30 S. F. Boys and F. Bernardi, *Mol. Phys.*, 1970, **19**, 553.
- 31 M. J. Turner, J. J. McKinnon, S. K. Wolff, D. J. Grimwood, P. R. Spackman, D. Jayatilaka and M. A. Spackman, *Crystal Explorer (Version 17)*, University of Western Australia, Perth, Australia, 2017.
- 32 I. J. Bruno, J. C. Cole, P. R. Edgington, M. Kessler, C. F. Macrae, P. Mc Cabe, J. Pearson and R. Taylor, *Acta Crystallogr., Sect. B: Struct. Sci.*, 2002, **58**, 389.